14th International Workshop on Deep Inelastic Scattering, DIS2006, April 20-24, 2006, Tsukuba, Japan
www-h1.desy.de/h1/www/publications/conf/conf_list.html
H1prelim-06-011

Determination of diffractive parton densities by a combined analysis of diffractive dijetproduction and of the inclusive diffractive structure function F_2^D in deep inelastic scattering

H1 Collaboration

Abstract

Hard diffractive scattering processes in DIS are predicted to factorize into a process dependent hard QCD matrix element and diffractive parton distributions which are universal for processes such as inclusive deep inelastic scattering as described by the inclusive structure function $F_2^D(\beta, Q^2, x_{I\!P})$, jet production and production of heavy quarks. This QCD factorization is tested by a combined analysis of the differential dijet cross sections and F_2^D in next to leading order QCD. Differential twojet cross sections in diffractive deep inelastic scattering processes at low Q^2 have been measured with the H1 detector using an integrated luminosity of 51.5 pb^{-1}. Twojet events are identified using the inclusive k_T cluster algorithm in the $\gamma^\star - p$ rest frame. The cross sections are given at the level of stable hadrons and correspond to the kinematic range: $4\ \mathrm{GeV}^2 < Q^2 < 80\ \mathrm{GeV}^2$, $x_{I\!P} < 0.03$, $M_Y < 1.6$ GeV, $|t| < 1\ \mathrm{GeV}^2$, $p^\star_{\perp,jet1} > 5.5$ GeV, $p^\star_{\perp,jet2} > 4$ GeV, $-3 < \eta^\star_{jet} < 0$, where the $\star$ indicates the $\gamma^\star - p$ rest frame. Diffractive events are selected by requiring a rapidity gap between the central mass system X and the proton direction. Dijet cross sections are directly sensitive to the diffractive gluon distribution since their production is dominated by the photon-gluon fusion process whereas F_2^D is directly sensitive to the diffractive quark singlet distribution and only indirectly to the gluon distribution via the observed scaling violations. The diffractive gluon distributions are parameterized using an ansatz where they factorize into a pomeron flux which depends only on $x_{I\!P}$ and parton distributions which depend only on $z_{I\!P}$ and Q^2 as suggested by Regge theory. A subleading reggeon contribution is also added. Both data sets are compared to fixed order NLO QCD predictions and simultaneous fitted to the predictions of the DGLAP evolution equations leaving the parameters describing the diffractive quark and gluon distributions and the intercept of the pomeron flux factor free. Both data sets can be very well described by one set of parton distributions showing the validity of QCD factorization. This allows for the first time a very sensitive determination of both the diffractive quark and gluon distributions in the range $0.05 < z_{I\!P} < 0.9$.

1 Introduction

The study of hard diffraction processes at HERA has had a major impact on the understanding of diffraction and the structure of the 'Pomeron'. It has been demonstrated that hard diffractive processes like inclusive deep inelastic scattering (DIS) , jet production and production of charmed quarks can be well described by factorizing the cross section into a Pomeron flux and a hard QCD scattering process with a parton in the 'Pomeron' which is described by diffractive parton densities. Theoretically it is expected that the cross section $\sigma^D_{\rm incl}$ for inclusive diffractive deep-inelastic scattering (DIS) factorizes into universal diffractive parton distributions and process dependent hard scattering coefficients [1]. Diffractive parton densities have been determined from DGLAP QCD fits to inclusive diffractive HERA data [2, 3] and have been found to be dominated by the gluon distribution. Diffractive dijet production is directly sensitive to the gluon component of the diffractive exchange and has been shown- for DIS [4] - to be in decent agreement with the QCD fits to the inclusive diffractive data. In this paper, a measurement of diffractive dijet cross sections in deep inelastic scattering is presented, based on data collected with the H1 detector at HERA. The integrated luminosity is increased by a factor 5 with respect to previous results [4] and the data are taken at higher center of mass energy. Jets are defined using the inclusive k_T cluster algorithm with asymmetric cuts on the jet transverse energies to facilitate comparisons with next-to-leading order predictions. A combined NLO QCD fit is performed to the differential dijet cross sections and the inclusive diffractive structure function F_2^D in order to determine the diffractive quark and gluon distributions.

2 Kinematics

The main diagram leading to diffractive dijet production in DIS is shown in figure 1. The events are separated by the diffractive selection into a central hardonic system X with mass M_X which contains the two jets and a forward system Y which is limited to a mass $M_Y < 1.6$ GeV. The relevant kinematic variables used are the Bjørken variable $x = Q^2/Q^2_{max}$, Q^2 , the squared momentum transfer, the momentum fraction of the diffractive exchange $x_{I\!P}$ and the momentum fraction of the parton in the 'pomeron' $z_{I\!P}$. Jets are selected using the limited k_T algorithm in the $\gamma^\star - p$ system. They will be characterized by their transverse momentum $p^\star_\perp$ and their pseudo-rapidity η.

3 Diffractive parton distributions

In [3] diffractive parton distributions of the proton have been determined through DGLAP QCD fits to inclusive diffractive DIS data. The fits were made under the additional assumptions that the shapes of the parton distributions do not depend on $x_{I\!P}$ and their normalization is controlled through Regge phenomenology (resolved pomeron model). These assumptions are consistent with the present data. These parton densities are referred to as 'H1 2006 DPDF fit' in the present paper.

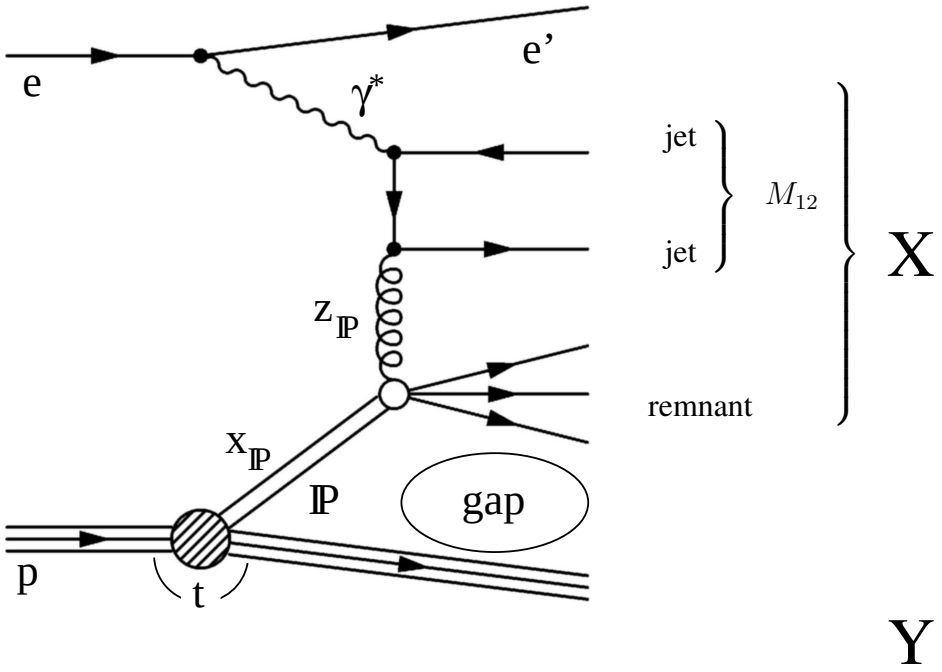

Figure 1: Leading diagram to diffractive 2-jet production in DIS at HERA.

4 Monte Carlo Simulations and Fixed Power QCD Predictions

In the analysis different Monte Carlo programs were used to correct the data for detector inefficiencies and migrations, and to compare the measured cross sections with model predictions. The RAPGAP 3.1 Monte Carlo program [5] is used to obtain predictions based on diffractive parton densities extracted in inclusive diffractive DIS within the resolved pomeron model. Leading order matrix elements for the hard QCD 2$\rightarrow$ 2 subprocess are convoluted with parton distributions of the pomeron, taken at the scale $\mu^2 = \hat{p}_T^2 + Q^2$, where $\hat{p}_T$ is the transverse momentum of the emerging hard partons and Q^2 the invariant mass of the virtual photon.

For the diffractive exchange, a preliminary version of the H1 2006 DPDF fit parameterizations is used to simulate pomeron and sub-leading reggeon exchange, which contributes at the highest $x_{I\!P}$. Higher order effects are simulated using parton showers [8] in the leading log(μ) approximation (MEPS), and the Lund string model [9] is used for hadronization. Radiative corrections are applied using the HERACLES program.

Fixed order QCD predictions at parton level for the dijet cross sections are calculated using the nlojet++ program [10] in slices of $x_{I\!P}$ making use of QCD factorization. QCD predictions for the measured inclusive structure function F_2^D of H1 [3] are obtained by a NLO QCD evolution program [11] which is also used for the stand alone QCD analysis of F_2^D.

5 Experimental Procedure

5.1 H1 Detector

A detailed description of the H1 detector can be found in [12, 13]. Here, a brief account of the components most relevant to the present analysis is given. The H1 coordinate system convention defines the outgoing proton beam direction as the positive z axis and the polar scattering angle θ such that the pseudo-rapidity $\eta = -\ln\tan(\theta/2)$ increases along z.

The hadronic final state X is measured with a tracking and a calorimeter system. The central ep interaction region is surrounded by two large concentric drift chambers, located inside a 1.15 T solenoidal magnetic field. Charged particle momenta are measured in the range $-1.5 < \eta < 1.5$ with a resolution of $\sigma/p_T = 0.01\,p_T/\text{GeV}$. A finely segmented electromagnetic and hadronic liquid argon calorimeter (LAr) covers the range $-1.5 < \eta < 3.4$. The energy resolution is $\sigma/E = 0.11/\sqrt{E/\text{GeV}}$ for electromagnetic showers and $\sigma/E = 0.50/\sqrt{E/\text{GeV}}$ for hadrons, as measured in test beams. A lead/scintillating fibre calorimeter (SPACAL) covers the backward region $-4 < \eta < -1.4$. The forward region is covered by the Forward Muon Detector (FMD) and the Proton Remnant Tagger (PRT). The 3 pre-toroid drift chambers of the FMD are used to detect particles directly in the region $1.9 < \eta < 3.7$, and from larger pseudo-rapidities via beam-pipe scattering. The PRT consists of a set of scintillators surrounding the beam pipe at $z = 26$ m and covers the region $6 < \eta < 7.5$. The ep luminosity is measured via the Bethe-Heitler Bremsstrahlung process $ep \to ep\gamma$, the final state electron and photon being detected in crystal calorimeters at $z = -33$ m (electron detector) and $z = -103$ m (photon detector), respectively.

5.2 Event Selection

The data used in this analysis were taken in the 1999 and 2000 running periods, in which HERA collided 920 GeV protons with 27.5 GeV positrons. The data are collected using a trigger which requires the scattered electron to be measured in the SPACAL calorimeter and at least 1 track of transverse momentum > 0.8 GeV in the central jet chamber. The scattered positron is required to be measured in the backward electromagnetic calorimeter with an energy $E_{e'} > 8$ GeV. The kinematic range is chosen to be $4\ \text{GeV}^2 < Q^2 < 80\ \text{GeV}^2$ and $0.1 < y < 0.7$.

Jets are formed from the tracks and clusters of the hadronic final state , using the inclusive k_T cluster algorithm [14] (with a distance parameter of 1.0) in the $\gamma^\star p$ system. Two jets are required, with transverse energies $p^\star_{\perp,1} > 5.5$ GeV and $p^\star_{\perp,2} > 4$ GeV for the leading and subleading jet, respectively. The jet axes are required to lie within the region $-1 < \eta_{jet} < 2.0$, well within the acceptance of the LAr calorimeter. Diffractive events are selected by requiring a rapidity gap using the forward H1 detectors. The maximum value for the rapidity of a significant energy deposition is required to be $\eta_{max} < 3.2$. In addition $x_{I\!P}$ is restricted to $x_{I\!P} < 0.03$. After all cuts we are left with 2723 twojet events. This is a very large statistical improvement compared to earlier studies [4].

Cross Section Definition

$4\ \mathrm{GeV}^2$	$<$	Q^2	$<$ $80\ \mathrm{GeV}^2$
0.1	$<$	y	$<$ 0.7
		$x_{I\!P}$	$<$ 0.03
		M_Y	$<$ $1.6\ \mathrm{GeV}$
		$\lvert t\rvert$	$<$ $1\ \mathrm{GeV}^2$
		$p^\star_{\perp,jet1}$	$>$ $5.5\ \mathrm{GeV}$
		$p^\star_{\perp,jet2}$	$>$ $4\ \mathrm{GeV}$
-3	$<$	$\eta^\star_{jet}$	$<$ 0

Table 1: The kinematic domain in which the cross sections are measured at the level of stable hadron jets. The jets are reconstructed using the inclusive k_T algorithm with the distance parameter set to 1.0.

5.3 Kinematic Reconstruction

The energy $E_{e'}$ and angle θ_e are measured directly in the SPACAL and is used to reconstruct the fractional photon energy y and photon virtuality Q^2 , as well as the mass of the hadronic system W:

$$y = 1 - \frac{E_{e'}}{E_e}\sin^2(\frac{\theta_e}{2}), \tag{1}$$

$$Q^2 = 4E_{e'}E_e\cos^2(\frac{\theta_e}{2}), \tag{2}$$

$$W^2 = ys - Q^2. \tag{3}$$

where E_e is the electron beam energy and s the CMS energy of the collision. The hadronic system X, containing the jets, is measured in the LAr and SPACAL calorimeters and the central tracking system. Calorimeter cluster energies and track momenta are combined using algorithms which avoid double counting [15]. $x_{I\!P}$ is reconstructed according to

$$x_{I\!P} = \frac{M_X^2 + Q^2}{W^2 + Q^2} \tag{4}$$

in which M_X denotes the invariant mass of the X system. The estimator $z_{I\!P}$ on the fractional momenta of the partons entering the hard subprocess is reconstructed from the mass of the dijet system M_{12} as:

$$z_{I\!P} = \frac{M_{12}^2 + Q^2}{M_X^2 + Q^2}. \tag{5}$$

5.4 Cross Section Measurement

The measured differential jet cross sections are defined at the level of stable hadrons. The data are corrected for detector inefficiencies and migrations of kinematic quantities in the reconstruction using the RAPGAP31 Monte Carlo program. For generated events, the H1 detector

response is simulated in detail and the Monte Carlo events are subjected to the same analysis chain as the data. The simulations give a very good description of the shapes of all data distributions.

The kinematic region for which the cross sections are measured is given in table 1. An analysis of systematic uncertainties has been performed in which the sensitivity of the measurement to variations of the detector calibration and the Monte Carlo Models used for correction are evaluated. The dominant systematic error on the cross sections arises from the uncertainty in the LAr calorimeter energy scale and from the uncertainty of the corrections needed to go from detector jets to hadron level. Particularly large is the uncertainty due to the transition from a rapidity gap (on detector level) to diffraction ($x_{I\!P} < 0.03$ and $M_Y < 1.6$ GeV at hadron level). This leads to an overall uncertainty of the cross section between 15%(up) and 10%(down).

The resulting cross section as function of y, $x_{I\!P}$, $p^{\star}_{\perp,jet1}$ and $\Delta\eta$ is shown in Figure 2. While the prediction based on the H1 2006 DPDF fit clearly overestimated the cross section, there is reasonable agreement between the data and the H1 2006 DPDF fit B. The largest difference can be seen in y, a variable closely related to $z_{I\!P}$. Cross sections differential in $z_{I\!P}$ are shown in Figure 3 in comparison to NLO predictions based on the H1 2006 DPDF fit [3]. The large difference between the two predictions clearly shows the large uncertainty of the gluon at high $z_{I\!P}$ density as determined from F_2^D only. It also demonstrates the accuracy to be gained by the inclusion of the dijet data into a combined QCD analysis.

6 Combined NLO QCD fit to the dijet cross section and F_2^D

The following data sets are used to determine the diffractive quark singlet and gluon densities by a NLO QCD fit assuming the validity of QCD factorization. The differential dijet cross section in $z_{I\!P}$ is used in the fit in 4 bins of the scale variable $p_{\perp}^{\star 2} + Q^2$ to constrain the gluon density, where $p^{\star}_{\perp}$ is the transverse momentum of the hardest jet. These measured cross sections are shown in figure 4 for dijets at stable hadron level in the kinematic range defined by table 1. The inner error bars of the data points indicate the statistical errors, the outer error bars the sum of statistical and uncorrelated systematic errors added in quadrature. The yellow band gives the uncertainty due to correlated systematic effects. Also shown is the NLO prediction based on the final fitted parton densities. In addition the H1 measurements of $F_2^D(x_{I\!P}, z_{I\!P}, Q^2)$ in the range $Q^2 > 8.5$ GeV are used to constrain mainly the quark singlet contribution, the Pomeron flux and the size of the nonleading reggeon contribution. At small $z_{I\!P}$ the rather large measured scaling violations give also good constraints of the gluon distribution. The F_2^D measurements are shown in figures 5-8 together with the final NLO prediction.

In the first fit step the quark and gluon distributions are evolved from parameterized starting distributions at a scale Q_0^2 to the full Q^2 range using a NLO QCD evolution program [11] and then predictions for F_2^D are calculated. In a second step these diffractive parton densities are used to predict the differential dijet cross sections using the nlojet++ program. This second step would be very time consuming if it would be repeated for every fit step. The nlojet++ predictions are therefore calculated only once for a large range of values in the variables $z_{I\!P}$,$x_{I\!P}$ and bins in the scale $p_{\perp}^2 + Q^2$ for the different parton flavours and stored in matrix form. The predictions for the cross section during the fit are then obtained by summing up all cross section

contributions obtained from interpolation in this matrix. This procedure has been shown to agree with direct nlojet++ predictions to better than 2% in the fit range. The parton distributions are parameterized following the fit procedure for F_2^D as a product of a pomeron flux factor and parton densities of the pomeron: $xG_{I\!P}(x_{I\!P}, \beta, Q^2) = f_{I\!P}(x_{I\!P}) \cdot xG_{I\!P}(\beta, Q^2)$, where the flux-factor $f(x_{I\!P})$ is parameterized according to Regge phenomenology as $f_{I\!P}(x_{I\!P}) = 1./x_{I\!P}^{(\alpha(0)+\alpha' \cdot t)}$. To properly describe the data expecially at high $x_{I\!P}$ it is necessary to include the subleading exchange (the so called reggeon), so that:

$$xG(x_{I\!P}, \beta, Q^2) = f_{I\!P}(x_{I\!P}) \cdot xG_{I\!P}(\beta, Q^2) + f_{I\!R}(x_{I\!P}) \cdot xG_{I\!R}(\beta, Q^2) \tag{6}$$

The exact quantity measured in [3] is $x_{I\!P}\sigma_r^{D(3)}(x_{I\!P}, \beta, Q^2)$, where $\sigma_r^{D(3)}$ is the so called reduced cross section defined by:

$$\frac{d^3\sigma_{ep\to eXY}}{dx_{I\!P} d\beta dQ^2} = \frac{4\pi\alpha_{em}^2}{\beta^2 Q^4} \cdot Y_+ \cdot \sigma_r^{D(3)}(x_{I\!P}, \beta, Q^2), \tag{7}$$

where $Y_\pm = 1 \pm (1-y)^2$. In leading order the reduced cross section is identical to $F_2^{D(3)}$. The high precision of the measurement, however, compels a more sophisticated treatment, which leads to a description of $\sigma_r^{D(3)}$ in terms of three diffractive structure functions $F_2^{D(3)}$, $F_L^{D(3)}$ and $xF_3^{D(3)}$, similar to inclusive DIS [11]:

$$\sigma_r^{D(3)} = F_2^{D(3)} - \frac{y^2}{Y_+} F_L^{D(3)} - \frac{Y_-}{Y_+} xF_3^{D(3)}. \tag{8}$$

All of the three structure functions are computed to next to leading order from the parton densities by the QCDFIT program. The small reggeon contribution is fixed for the fit both in shape and magnitude to values obtained from a standalone F_2^D fit. The value of the strong coupling constant is fixed to $\alpha_s(m_Z)$= 0.1185. The Regge intercept $\alpha(0)$ of the pomeron flux factor on the other hand is left as a free parameter for the fit as well as all parameters which determine the shape and size of the parton distributions. The fit has a high probability as shown by the overall value χ^2/df = 0.89 which splits into χ^2/df = 27/36 for the dijet cross sections and χ^2/df = 169/190 for F_2^D. The value of $\alpha(0)$ obtained is 1.154. The diffractive gluon distribution and the quark singlet distribution are shown in figure 9 for a hard scale $\mu^2 = 25$ GeV^2 and $\mu^2 = 90$ GeV^2. The error bands indicate the preliminary systematic experimental errors. The combined fit for the first time constrains both the diffractive gluon and quark densities remarkably well in the range $0.05 < z_{I\!P} < 0.9$.

Dijet cross sections compared to the predictions based on the combined fit are shown in figures 4 and 10. The error bands of the NLO predictions are scale errors obtained by varying the renormalization and factorization scale μ in the QCD prediction by a factor 2 and 0.5 respectively. There is reasonable overall agreement for all distributions which underlines that a consistent NLO QCD prediction is possible by a suitable choice of the diffractive parton distributions. Figures 5–8 show the measurements of F_2^D versus Q^2 for different bins in $x_{I\!P}$ together with the NLO predictions based on the final parton distributions of the combined fit. Again a very good description is obtained which is also reflected in the resulting values χ^2/ndf given above. We therefore conclude that our data is in agreement with QCD factorization since both data sets can be consistently described by the same diffractive parton densities. It has been checked that a fit to the inclusive structure function alone gives adequately consistent results

with earlier analyses [3]. Not all desirable systematic studies have been performed yet however, the error band for the parton distributions is therefore only preliminary and probably too optimistic. Also the effect of changes in the hard QCD scale are not yet included.

7 Summary

The measurement of diffractive dijet cross sections with rather high statistical accuracy allows to directly determine the diffractive gluon density in combination with the inclusive diffractive structure function F_2^D which mainly determines the the quark singlet distribution, the pomeron flux and the size of the nonleading reggeon contribution. A NLO QCD DGLAP evolution is able to describe both the shape and scaling violations of F_2^D and the dijet cross sections consistently. We therefore conclude that QCD factorization in DIS is valid in our kinematic region. The data has allowed for the first time to determine both the diffractive gluon and the singlet quark distribution with good accuracy in the range $0.1 < z_{I\!P} < 0.9$.

Acknowledgements

We are grateful to the HERA machine group whose outstanding efforts have made and continue to make this experiment possible. We thank the engineers and technicians for their work in constructing and now maintaining the H1 detector, our funding agencies for financial support, the DESY technical staff for continual assistance, and the DESY directorate for the hospitality which they extend to the non DESY members of the collaboration.

References

[1] J. Collins, Phys. Rev. **D57** (1998) 3051 and erratum-ibid. **D61** (2000) 019902.

[2] C. Adloff *et al.* [H1 Collaboration], Z. Phys. **C76** (() 1997) 613

[3] H1prelim-01-111

[4] H1prelim-04-113

[5] H. Jung, *Hard diffractive scattering in high-energy e p collisions and the Monte Carlo generation RAPGAP*, Comput. Phys. Commun. **86** (1995) 147.

[6] M. Gluck, E. Reya and A. Vogt, Phys. Rev. D **45** (1992) 3986.
M. Gluck, E. Reya and A. Vogt, Phys. Rev. D **46** (1992) 1973.

[7] C. Adloff *et al.* [H1 Collaboration], Phys. Lett. B **483** (2000) 36 [arXiv:hep-ex/0003011].

[8] M. Bengtsson and T. Sjostrand, Z. Phys. C **37** (1988) 465.

[9] B. Andersson, *The Lund String Model*, aus Durham 1984, Proceedings, Antiproton 1984, 447-462.

[10] Z. Nagy and Z. Trocsanyi, Phys. Rev. Lett. **87** (2001) 082001 [arXiv:hep-ph/0104315].

[11] M. Botje, M. Klein and C. Pascaud, arXiv:hep-ph/9609489.

[12] I. Abt *et al.* [H1 Collaboration], Nucl. Instrum. Meth. A **386** (1997) 310.

[13] I. Abt *et al.* [H1 Collaboration], Nucl. Instrum. Meth. A **386** (1997) 348.

[14] S. D. Ellis and D. E. Soper, Phys. Rev. D **48** (1993) 3160 [arXiv:hep-ph/9305266].
S. Catani, Y. L. Dokshitzer, M. H. Seymour and B. R. Webber, Nucl. Phys. B **406** (1993) 187.

[15] C. Adloff *et al.* [H1 Collaboration], Z. Phys. C **74** (1997) 221 [arXiv:hep-ex/9702003].

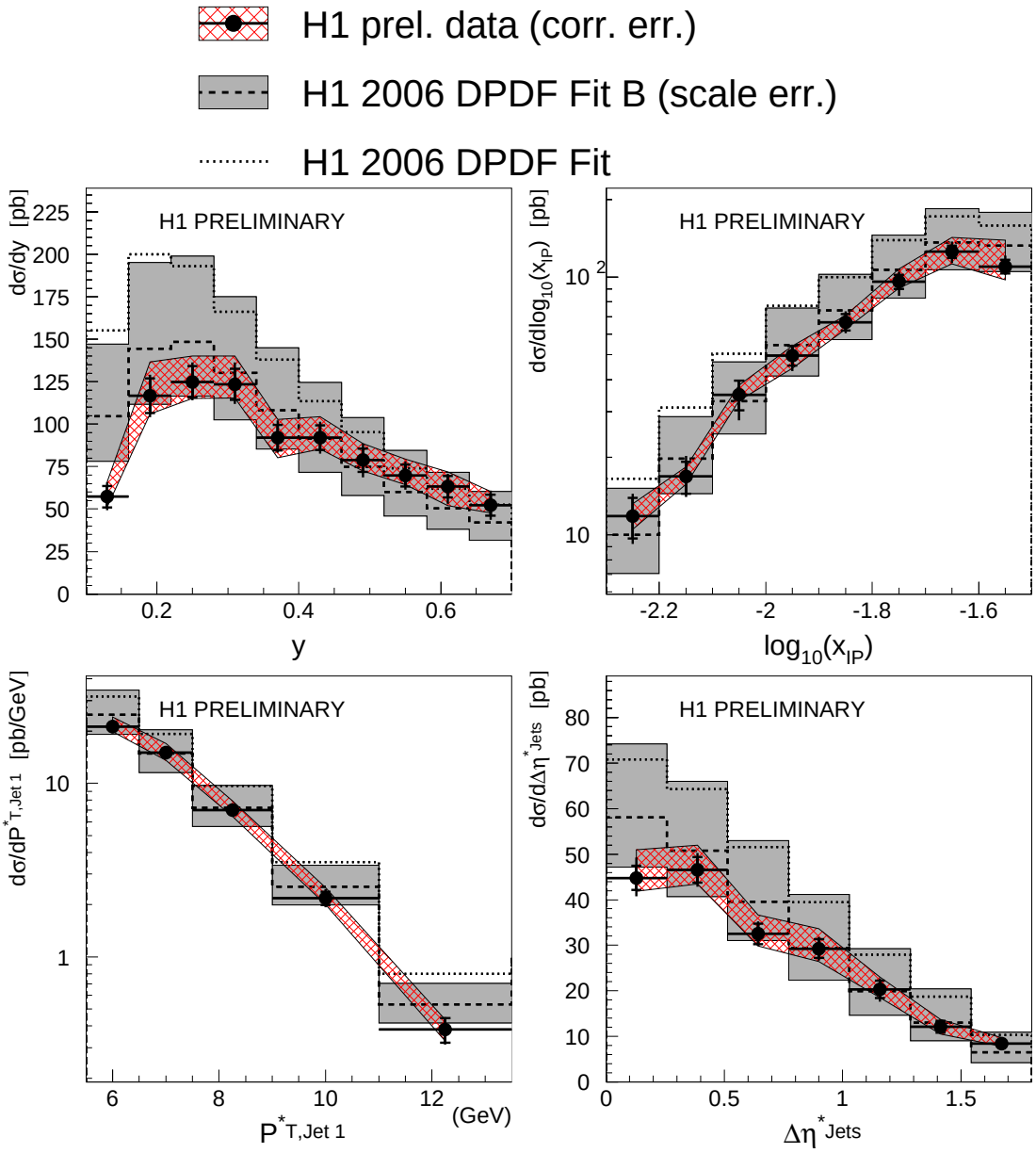

Figure 2: Cross section of diffractive dijets differential in Q^2, $p^{\star}_{\perp,jet1}$, y and $\Delta\eta$ compared to NLO predictions based on the parton-densities from the H1 2006 DPDF fit [3]. The data are shown as black points with the inner and outer error-bar denoting the statistical and uncorrelated systematic uncertainties respectively. The red hatched band indicates the correlated systematic uncertainty. The black dashed line shows the NLO QCD prediction based on the H1 2006 DPDF fit B surrounded by a grey band indicating the scale uncertainty. The black dotted line represents the NLO QCD prediction based on the H1 2006 DPDF fit.

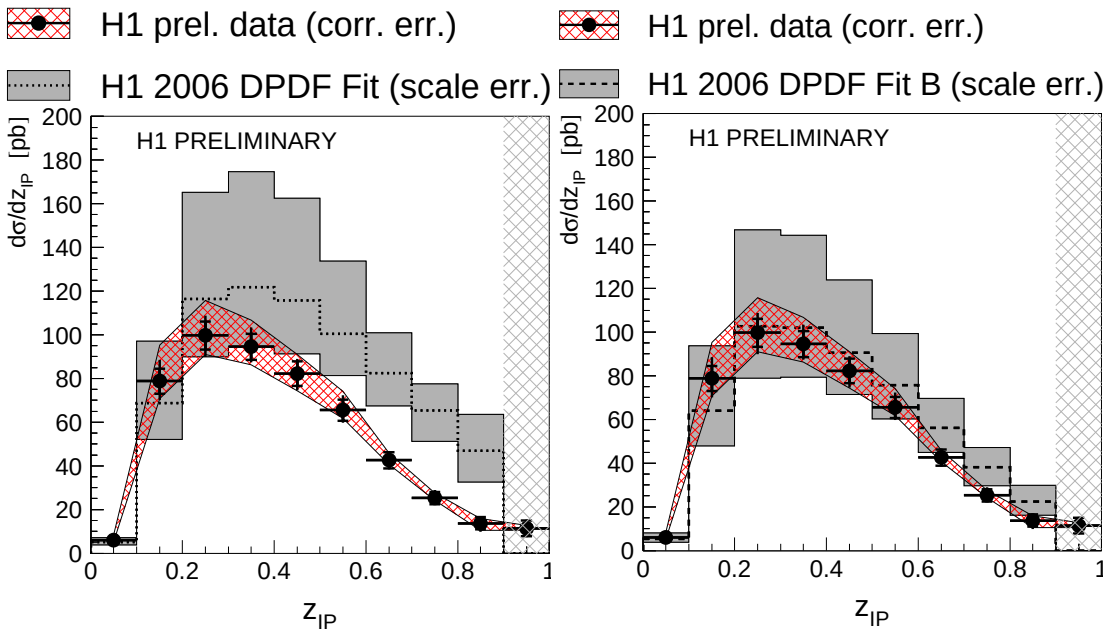

Figure 3: Cross section of diffractive dijets differential in $z_{I\!P}$ compared to NLO predictions based on the parton-densities from the H1 2006 DPDF fit [3]. The data are shown as black points with the inner and outer error-bar denoting the statistical and uncorrelated systematic uncertainties respectively. The red hatched band indicates the correlated systematic uncertainty. The black line shows the NLO QCD prediction based on the H1 2006 DPDF fit (left) and H1 2006 DPDF fit B (right) and is surrounded by a grey band indicating the scale uncertainty. The prediction for $z_{I\!P} > 0.9$ was set to zero due to problems with the hadronization corrections.

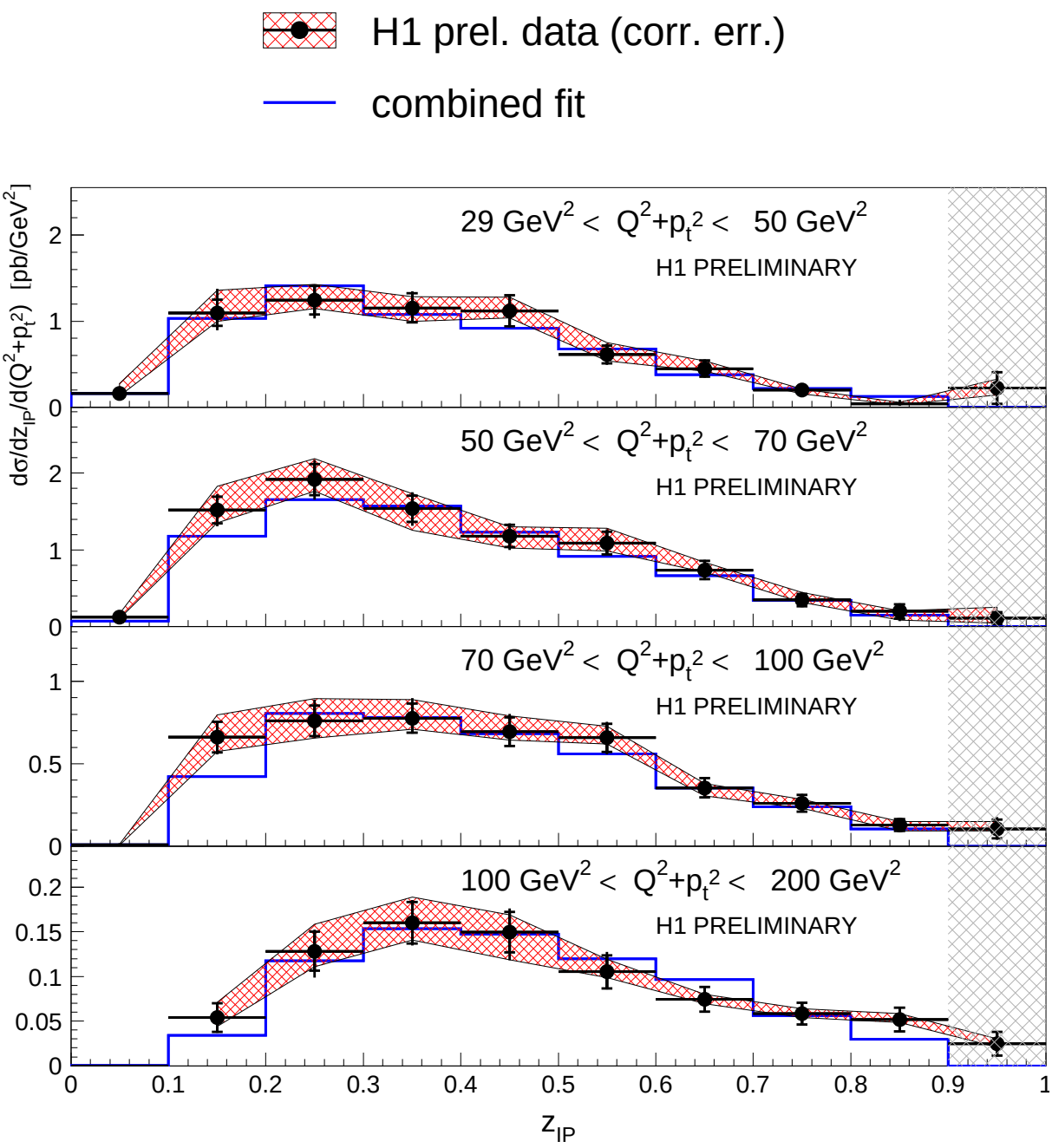

Figure 4: Cross section of diffractive dijets doubly differential in in $z_{I\!P}$ and the scale $\mu = Q^2 + p_\perp^{star2}$. The data are shown as black points with the inner and outer error-bar denoting the statistical and uncorrelated systematic uncertainties respectively. The red hatched band indicates the correlated systematic uncertainty. The blue line shows the NLO QCD prediction based on the combined fit. Data points in the grey hatched area were not included in the fit due to problems with the hadronization corrections.

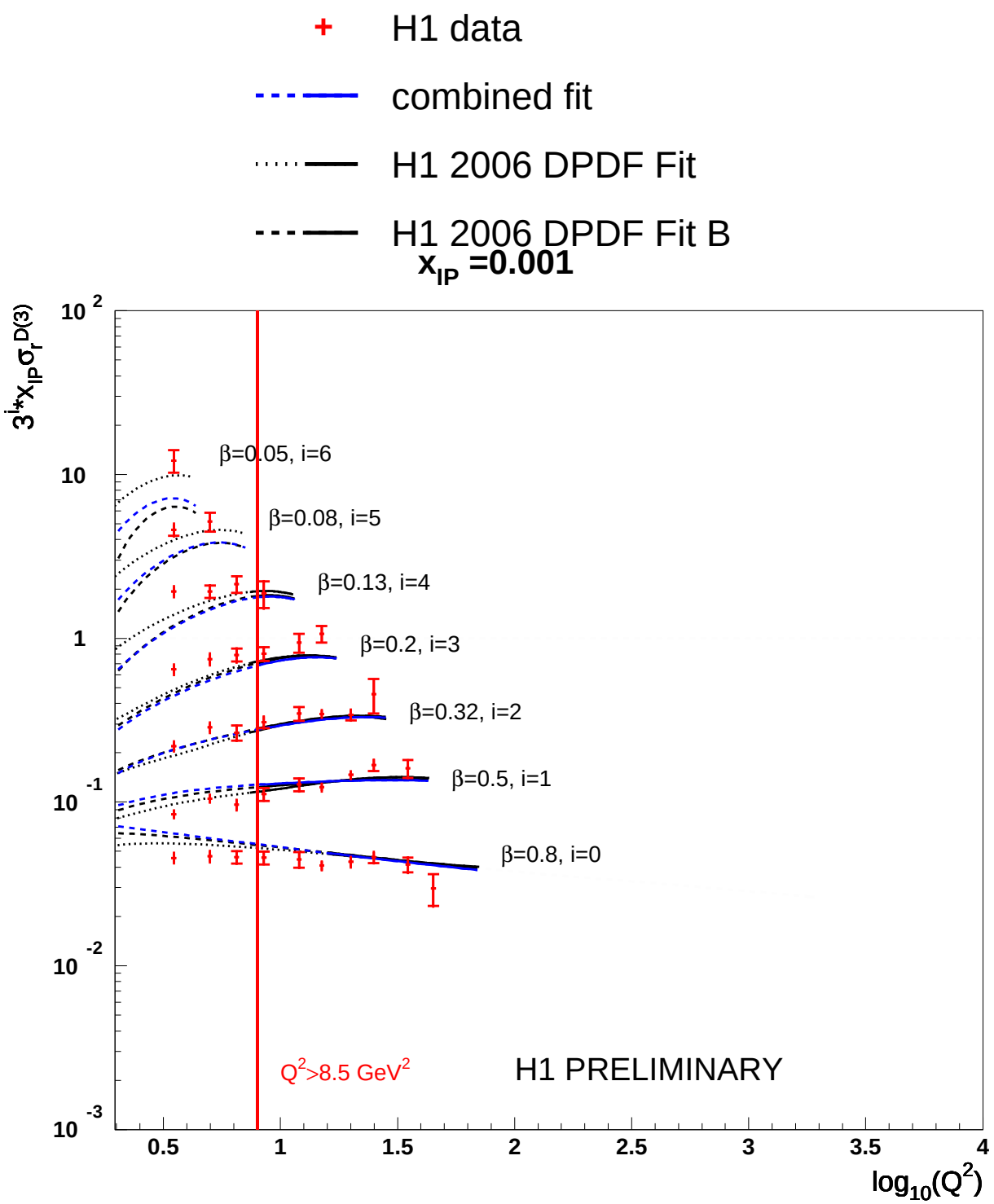

Figure 5: The β and Q^2 dependence of the diffractive reduced cross section $\sigma_r^{D(3)}$ multiplied by $x_{I\!P}$ at $x_{I\!P}$ =0.001. The cross sections are multiplied by powers of 3 for better visibility. The inner and outer error-bars on the data points represent the statistical and total uncertainties, respectively. The data are compared to the results of the combined fit for $E_p = 820$ GeV, which is shown as blue lines. The dashed line indicates the prediction in kinamtic regions that did not enter into the fit. The two black lines indicate the predictions of the H1 2006 DPDF fit.

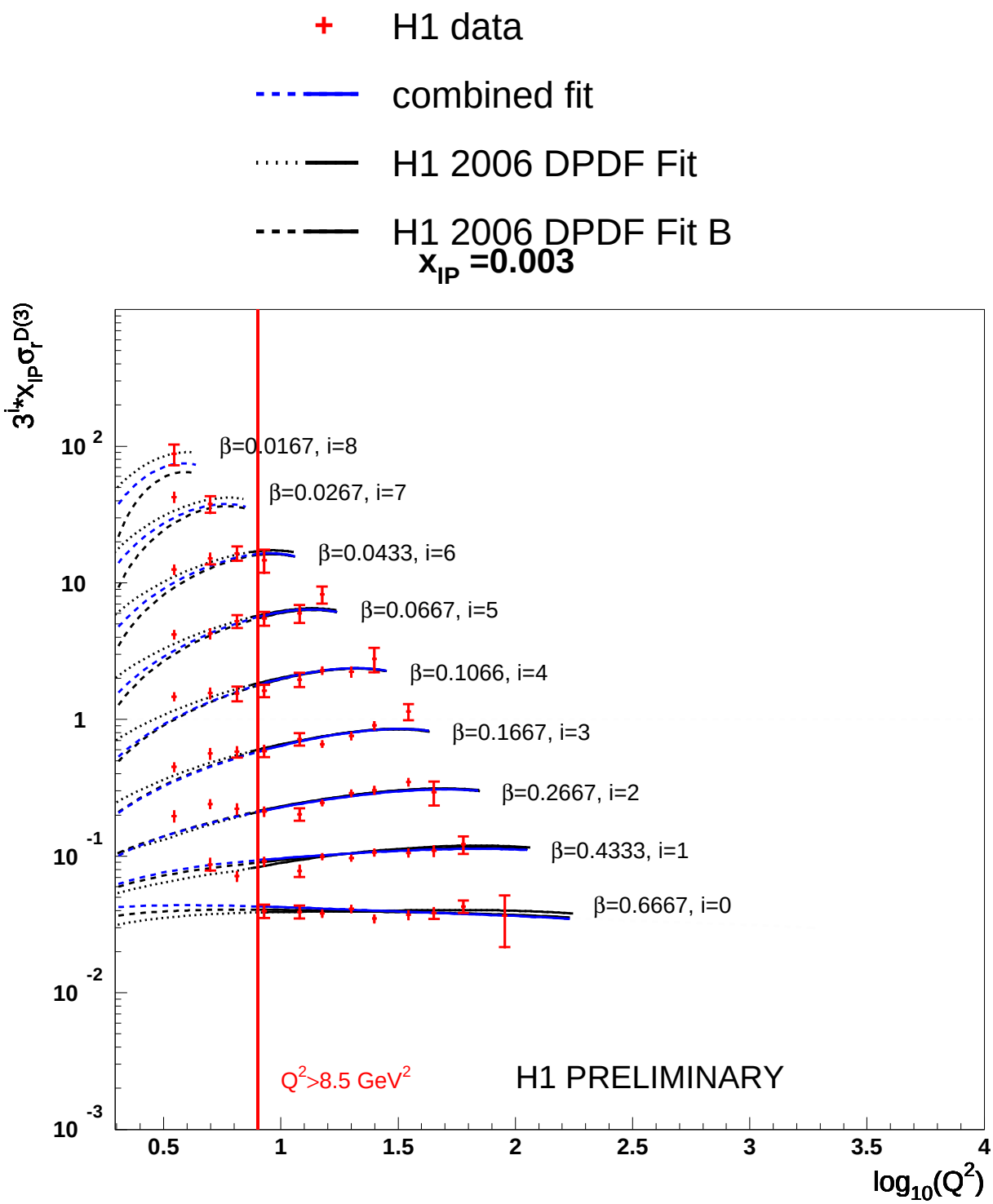

Figure 6: The β and Q^2 dependence of the diffractive reduced cross section $\sigma_r^{D(3)}$ multiplied by $x_{I\!P}$ at $x_{I\!P}$ =0.003. See caption of figure 5 for further details.

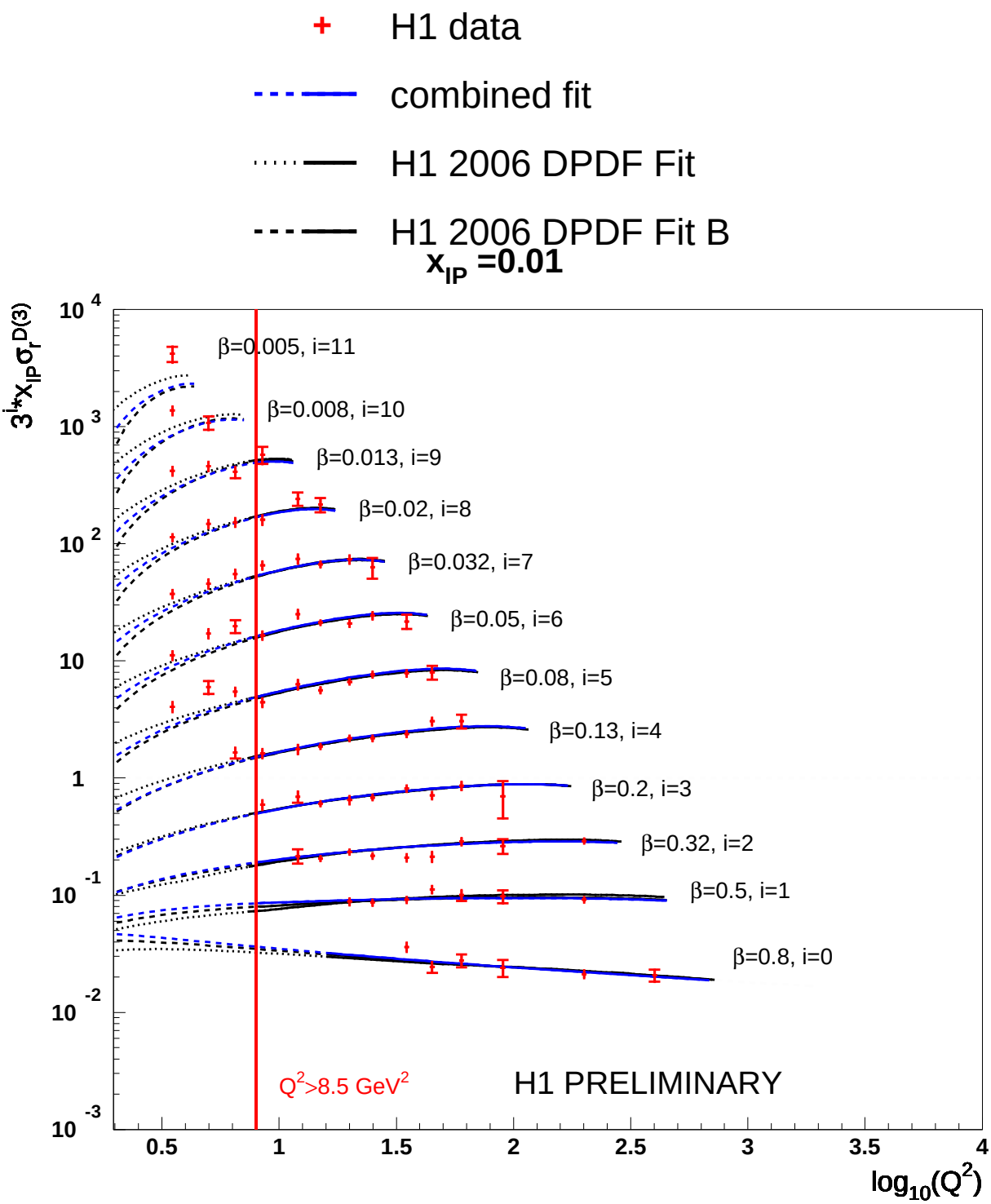

Figure 7: The β and Q^2 dependence of the diffractive reduced cross section $\sigma_r^{D(3)}$ multiplied by $x_{I\!P}$ at $x_{I\!P}$ =0.01. See caption of figure 5 for further details.

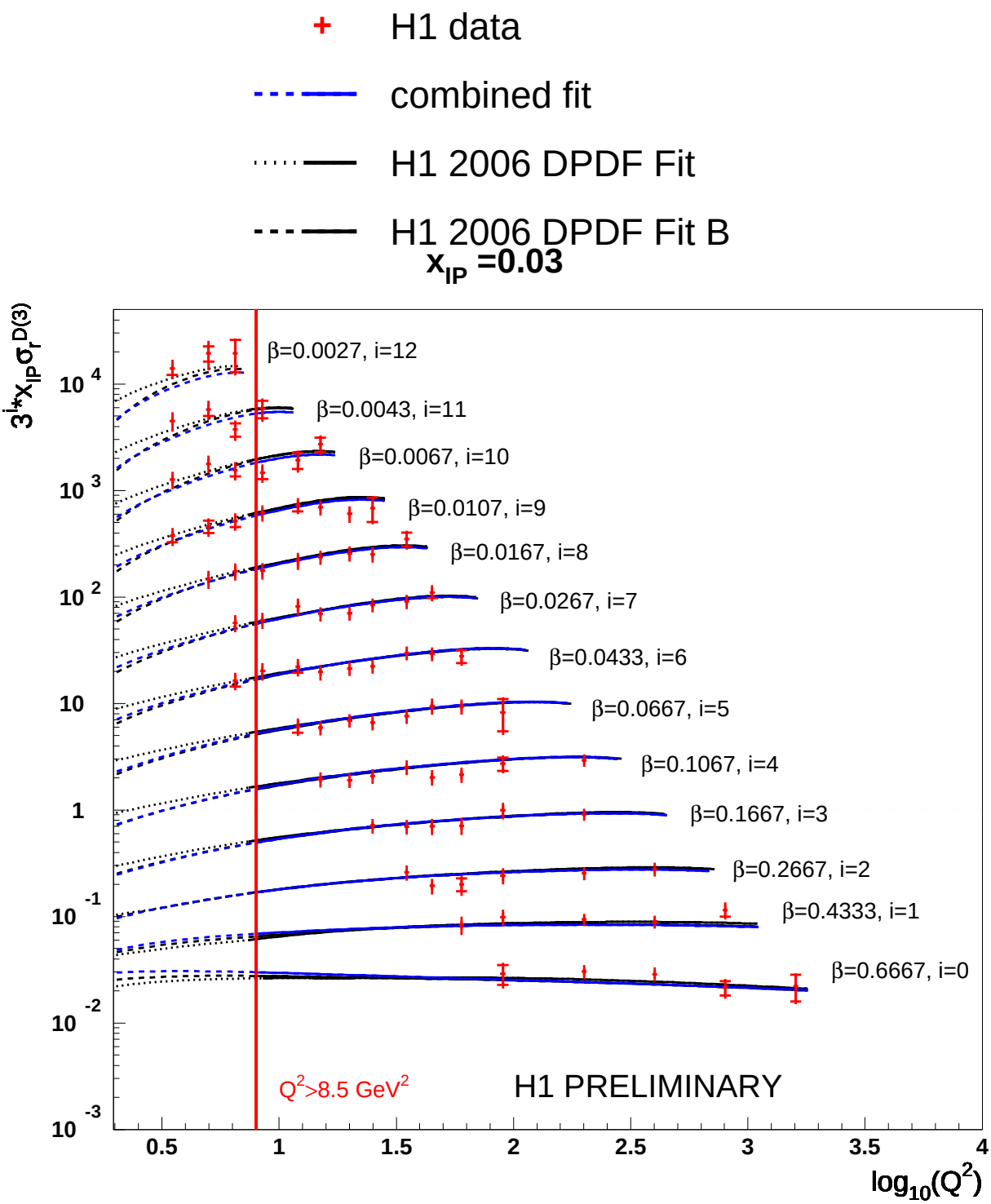

Figure 8: The β and Q^2 dependence of the diffractive reduced cross section $\sigma_r^{D(3)}$ multiplied by $x_{I\!P}$ at $x_{I\!P}$ =0.03. See caption of figure 5 for further details.

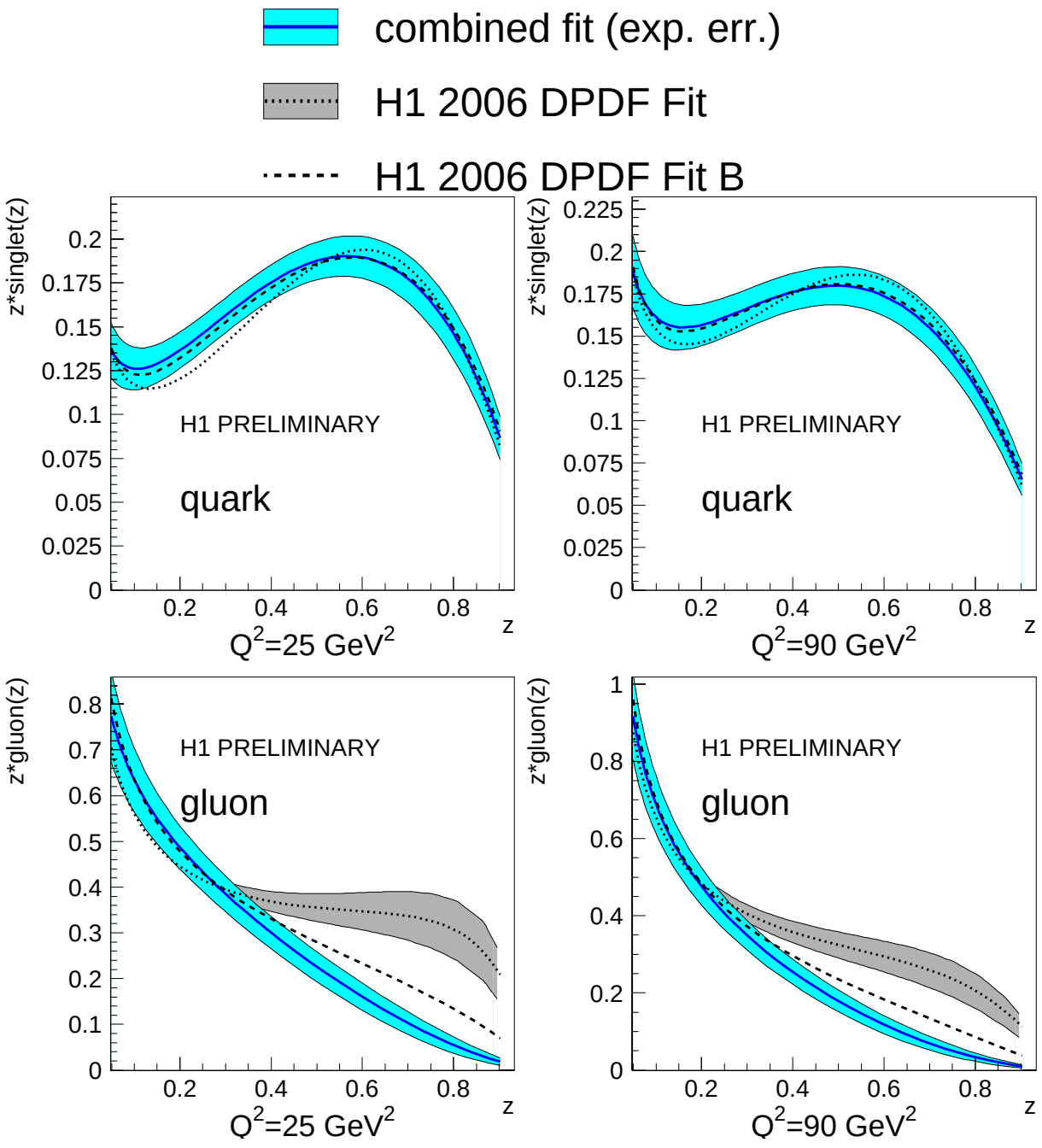

Figure 9: The diffractive singlet density (top) and diffractive gluon density (bottom) for two values of the hard scale μ: 25 GeV^2 (left) and 90 GeV^2 (right). The blue line indicates the combined fit, sourrounded by the experimental uncertainty band in light blue. The two dashed lines show the two fit results from 5 for comparison.

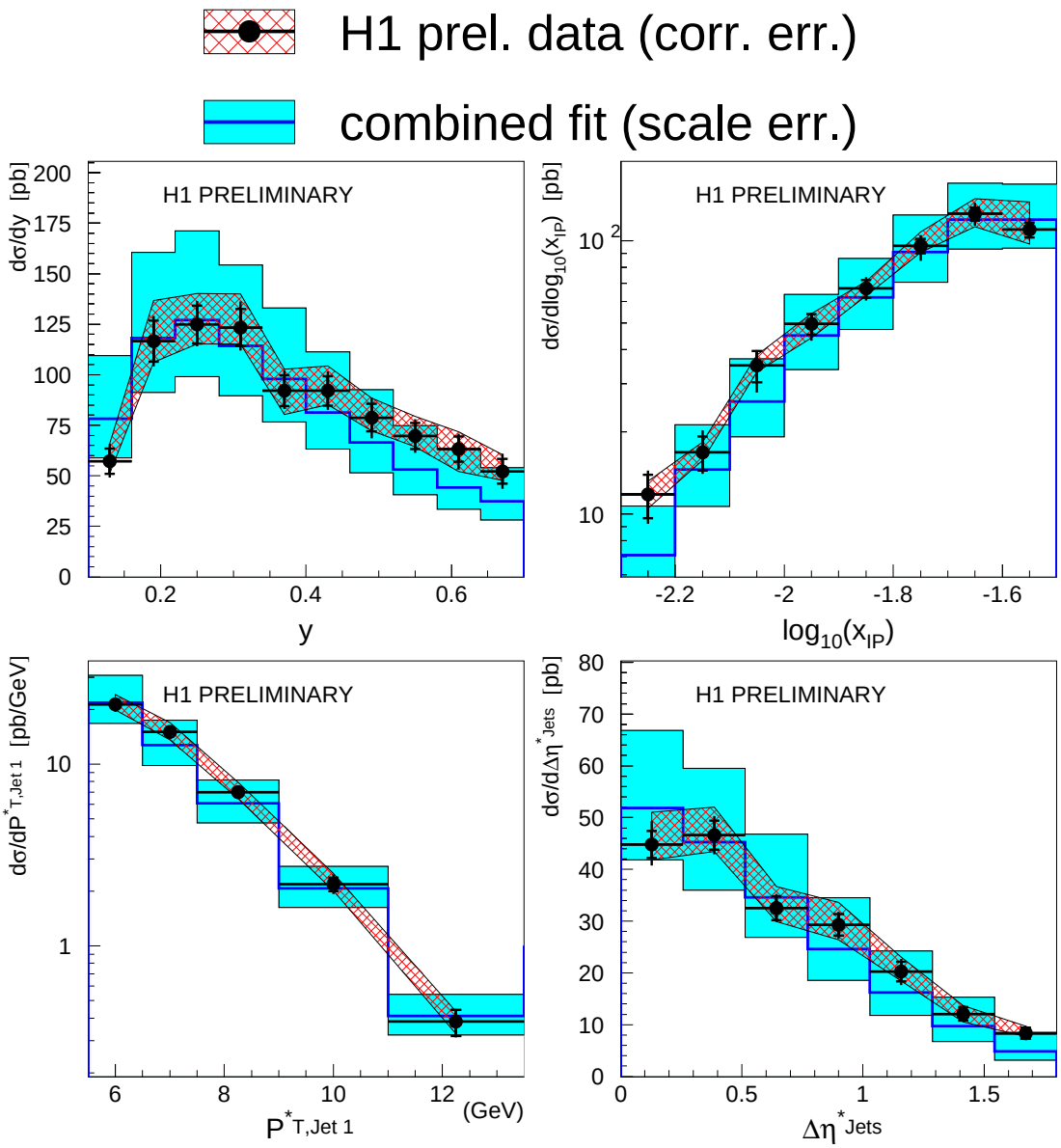

Figure 10: Differential cross sections of the dijet data in the variables y, $x_{I\!P}$, $p^{\star}_{\perp,1}$ and $|\eta^{\star}_1 - \eta^{\star}_2|$. The data are shown as black points with the inner and outer error-bar denoting the statistical and uncorrelated systematic uncertainties respectively. The red hatched band indicates the correlated systematic uncertainty. The blue line surrounded by the shaded band shows the NLO QCD prediction based on the combined fit, where the band denotes the scale uncertainty derived by varying μ by factors of 2 and 0.5.